Available online at www.sciencedirect.com
ScienceDirect
Trans. Nonferrous Met. Soc. China 26(2016) 2617−2632
Transactions of Nonferrous Metals Society of China
www.tnmsc.cn

Effects of aspect ratio and loading rate on room-temperature mechanical properties of Cu-based bulk metallic glasses

An-hui CAI[1,2,3], Yong LIU[2], Hong WU[2], Da-wei DING[3], Wei-ke AN[1],
Guo-jun ZHOU[1], Yun LUO[1], Yong-yi PENG[4], Xiao-song LI[1]

1. College of Mechanical Engineering, Hunan Institute of Science and Technology, Yueyang 414000, China;
2. State Key Laboratory of Powder Metallurgy, Central South University, Changsha 410083, China;
3. Institute of Physics, Chinese Academy of Sciences, Beijing 100190, China;
4. School of Physics and Electronics, Central South University, Changsha 410083, China

Received 16 October 2015; accepted 2 May 2016

Abstract: Room-temperature mechanical properties of $Cu_{50}Zr_{40}Ti_{10-x}Ni_x$ ($0\le x\le 4$, mole fraction, %) bulk metallic glasses (BMG) with aspect ratios in the range of 1:1−2.5:1 and loading rates in the range of 1×10^{-5}−1×10^{-2} s^{-1} were systematically investigated by room-temperature uniaxial compression test. In the condition of an aspect ratio of 1:1, the superplasticity can be clearly observed for $Cu_{50}Zr_{40}Ti_{10}$ BMG when the loading rate is 1×10^{-4} s^{-1}, while for $Cu_{50}Zr_{40}Ti_{10-x}Ni_x$ (x=1−3, mole fraction, %) BMGs when the loading rate is 1×10^{-2} s^{-1}. The plastic strain (ε_p), yielding strength (σ_y) and fracture strength (σ_f) of the studied Cu-based BMGs significantly depend on the aspect ratio and the loading rate. In addition, the σ_y of the studied Cu-based BMGs with an aspect ratio of 1:1 is close to the σ_f of those with the other aspect ratios when the loading rate is 1×10^{-2} s^{-1}. The mechanism for the mechanical response to the loading rate and the aspect ratio was also discussed.

Key words: Cu-based bulk metallic glasses; aspect ratio; loading rate; plasticity; strength

1 Introduction

Cu−Zr−Ti ternary alloys are one of Cu−Zr-based glass forming alloys. Critical diameter (d_c) and plastic strain (ε_p) of Cu−Zr−Ti BMGs can reach up to 5 mm [1] and 7.4% [2], respectively. Recently, CAI et al [3−8] have found that structural, thermal and corrosive performances of $Cu_{60-x}Zr_{30+x}Ti_{10}$ (x=0, 5, 10, mole fraction, %) metallic glasses can be significantly changed after the tension/compression. $Cu_{50}Zr_{40}Ti_{10}$ metallic glass characterizes in good deformability [6,7] and low hardness [8] among $Cu_{60-x}Zr_{30+x}Ti_{10}$ (x=0, 5, 10, mole fraction, %) metallic glasses, but its critical dimension and plastic strain are only 2 mm and 1.5% [9], respectively. Interestingly, the glass forming ability, mechanical, electrical and thermal properties can be simultaneously improved for Cu−Zr−Ti glass forming alloys by Ni addition [10−12]. For example, WU et al [11] fabricated a monolithic $Cu_{54.5}Zr_{37}Ti_8Ni_{0.5}$ BMG whose plastic strain and fracture strength can reach up to 26% and 2471 MPa, respectively.

It is well-known that the mechanical properties of the BMG are related with two kinds of factors. One is intrinsic factors such as the composition and/or microstructure of the BMG [10−17]. For example, WU et al [12] designed a $Cu_{51}Zr_{37}Ti_8Ni_4$ BMG which displays remarkable plasticity of 10.5% together with the fracture strength of 2145 MPa through the compositional regulation. LIU et al [15] designed three Zr-based BMGs with room-temperature compressive superplasticity due to the structural heterogeneity. The other is external factors, including the size [18−20], aspect ratio H/D (H and D are the height and the diameter of samples, respectively) [21−23], loading/strain rate [24−33], geometry [34,35], stress/strain state [36,37], and other factors [38−40]. The aspect ratio and the loading/strain rate are two important factors significantly influencing the mechanical properties of the BMG. ZHANG et al [21] and JIANG et al [22] found that the plastic strain

Foundation item: Projects (50874045, 51301194) supported by the National Natural Science Foundation of China; Project (2144057) supported by the Beijing Natural Science Foundation, China
Corresponding author: An-hui CAI; Tel: +86-730-8648848; E-mail: cah1970@sohu.com
DOI: 10.1016/S1003-6326(16)64388-1

increased with decreasing aspect ratio and the yield strength almost maintained a constant value. However, BRUCK et al [23] investigated the effect of two aspect ratios (1:2 and 2:1) on the compressive properties and found a slight increase in the yield strength with decreasing aspect ratio. In addition, it was found that the compressive strength decreased with increasing strain rate for $Zr_{38}Ti_{17}Cu_{10.5}Co_{12}Be_{22.5}$ BMG [28], $Zr_{57}Ti_5Cu_{20}Ni_8Al_{10}$ BMG [29], and $Pd_{40}Ni_{40}P_{20}$ BMG [31], respectively. The fracture strength was independent of the strain rate for $Zr_{41.25}Ti_{13.75}Cu_{12.75}Ni_{10}Be_{22.5}$ BMG in compression [32] and $Pd_{40}Ni_{40}P_{20}$ BMG in tension [30], respectively. However, the compressive strength was found to increase with increasing strain rate for $Ti_{40}Zr_{25}Ni_8Cu_9Be_{18}$ BMG [20] and $Nd_{60}Fe_{20}Co_{10}Al_{10}$ BMG [27], respectively. In addition, the dependence of the plastic and/or fracture strain of the BMG on the loading rate and the aspect ratio is similar to that of the mechanical properties. For example, the plastic and fracture strain were found to decrease with increasing strain rate for $Zr_{38}Ti_{17}Cu_{10.5}Co_{12}Be_{22.5}$ BMG [28], $Ti_{40}Zr_{25}Ni_8Cu_9Be_{18}$ BMG [20], $Ti_{45}Zr_{16}Ni_9Cu_{10}Be_{20}$ BMG [26], and $Nd_{60}Fe_{20}Co_{10}Al_{10}$ BMG [27] in compression, and increase with increasing strain rate for $Zr_{41.25}Ti_{13.75}Cu_{12.75}Ni_{10}Be_{22.5}$ BMG in tension [33], while they were independent of the strain rate for $Pd_{40}Ni_{40}P_{20}$ BMG in tension [31] and $Zr_{41.25}Ti_{13.75}Cu_{12.75}Ni_{10}Be_{22.5}$ BMG in compression [32], respectively. Interestingly, ZHANG et al [26] found little effect of the mechanical properties on the strain rate when the strain rate was below 1×10^{-3} s^{-1} and a positive strain rate dependence of yield strength when the strain rate was up to 1×10^{-1} s^{-1} for $Ti_{45}Zr_{16}Ni_9Cu_{10}Be_{20}$ BMG. In addition, both the strength and plasticity increased with increasing the strain rate up to a critical value, above which the strength and plasticity started to decrease for $Zr_{56}Al_{10.9}Ni_{4.6}Cu_{27.8}Nb_{0.7}$ BMG [24] and SrCaYbMg(Li)Zn(Cu) BMGs [25], respectively. Nevertheless, no reports for these problems can be found for Cu-based BMGs.

In the present work, the effects of the aspect ratio and the loading rate on the mechanical properties of $Cu_{50}Zr_{40}Ti_{10-x}Ni_x$ ($0\le x\le4$, mole fraction, %) BMGs were investigated by room-temperature compressive tests. It is found that the yield strength, fracture strength and plasticity significantly depend on the aspect ratio and the loading rate for the studied Cu-based BMGs.

2 Experimental

Master ingots of Cu−Zr−Ti−(Ni) alloys with normal compositions (in mole fraction, %), as shown in Table 1, were prepared by arc melting the mixture of ultrasonically cleaned high purity Cu (99.99%), Zr (99.99%), Ti (99.99%) and Ni (99.99%) in a Ti-gettered argon atmosphere. Then, *d*2 mm samples were prepared by suction casting into a water-cooled Cu mold.

The glassy natures of the as-cast samples were characterized by X-ray diffraction (XRD) using an

Table 1 Yielding strength σ_y, fracture strength σ_f, plastic strain ε_p, fracture strain ε_f, and $\varepsilon_p/\varepsilon_f$ under different aspect ratios and loading rates for $Cu_{50}Zr_{40}Ti_{10-x}Ni_x$ ($0\le x\le4$) bulk metallic glasses

x(Ni)/%	Aspect ratio	Loading rate/s^{-1}	σ_y/MPa	σ_f/MPa	ε_p/%	ε_f/%	$(\varepsilon_p/\varepsilon_f)$/%
0	1:1	1×10^{-2}	1860.3	1915.7	1.9	15.9	11.9
		1×10^{-3}	1720.5	1922.8	3.0	15.5	19.4
		1×10^{-4}	1877.1	Superhigh	Superhigh	Superhigh	100.0
		1×10^{-5}	1905.6	2449.2	14.5	29.5	49.2
	1.5:1	1×10^{-2}	1102.9	1259.6	2.3	9.6	24.0
		1×10^{-3}	1736.2	1917.6	1.4	9.4	14.9
		5×10^{-4}	1986.4	2049.6	1.6	10.7	15.0
		1×10^{-4}	1723.5	1911.2	2.5	12.9	19.4
		1×10^{-5}	1573.1	1755.1	2.6	10.7	24.3
	2:1	1×10^{-2}	1609.6	1978.2	3.3	10.4	31.7
		1×10^{-3}	1710.9	1923.9	2.1	10.7	19.6
		1×10^{-4}	1553.4	1880.6	2.4	9.4	25.5
		1×10^{-5}	1553.0	1860.3	2.5	8.5	29.4
	2.5:1	1×10^{-2}	−	1264.6	−	6.0	0
		1×10^{-3}	1615.7	1827.0	1.0	9.7	10.3
		1×10^{-4}	1671.3	1927.5	1.7	7.1	23.9
		1×10^{-5}	1632.0	1877.5	1.4	7.8	17.9

to be continued

Continued

x(Ni)/%	Aspect ratio	Loading rate/s^{-1}	σ_y/MPa	σ_f/MPa	ε_p/%	ε_f/%	$(\varepsilon_p/\varepsilon_f)$/%
0.5	1:1	1×10^{-2}	1936.1	2193.8	6.7	22.3	30.0
		1×10^{-3}	1879.9	2339.9	10.5	22.1	47.5
		1×10^{-4}	1956.5	2123.6	10.3	27.3	37.7
		1×10^{-5}	1908.0	1984.6	2.3	16.6	13.9
	1.5:1	1×10^{-2}	1880.3	2030.7	1.6	10.4	15.4
		1×10^{-3}	1723.5	1899.2	1.6	10.2	15.7
		1×10^{-4}	1792.4	1974.4	4.2	13.5	31.1
		1×10^{-5}	1779.9	1968.1	2.6	12.5	20.8
	2:1	1×10^{-2}	1623.0	1930.2	2.2	10.1	21.8
		1×10^{-3}	1661.1	1886.6	1.8	8.9	20.2
		1×10^{-4}	1729.8	1986.4	4.1	10.3	39.8
		1×10^{-5}	1717.2	1949.2	1.5	8.0	18.8
	2.5:1	1×10^{-2}	−	1679.9	−	5.9	0
		1×10^{-3}	1592.1	1886.6	1.7	8.2	20.7
		1×10^{-4}	1654.6	1936.5	3.6	10.6	34.0
		1×10^{-5}	1742.5	2037.0	4.0	14.5	27.6
1	1:1	1×10^{-2}	1866.6	Superhigh	Superhigh	Superhigh	100.0
		5×10^{-3}	1824.4	2242.3	11.0	24.1	45.6
		1×10^{-3}	1859.6	1956.5	2.2	16.6	13.3
		1×10^{-4}	1846.2	1866.6	0.5	15.2	3.3
		1×10^{-5}	−	1767.0	−	14.6	0
	1.5:1	1×10^{-2}	−	1824.0	−	8.0	0
		1×10^{-3}	1842.3	2099.6	3.0	14.3	21.0
		1×10^{-4}	1691.9	1949.2	2.2	11.4	19.3
		1×10^{-5}	1773.5	1923.9	2.0	11.6	17.2
	2:1	1×10^{-2}	1796.3	1936.1	1.5	9.2	16.3
		1×10^{-3}	1629.2	2256.3	9.3	18.2	51.1
		1×10^{-4}	1657.3	1998.6	4.5	12.9	34.9
		1×10^{-5}	1740.9	2005.6	3.8	11.7	32.5
	2.5:1	1×10^{-2}	1892.9	1968.1	0.5	7.7	6.5
		1×10^{-3}	1886.6	1942.8	0.4	6.5	6.2
		1×10^{-4}	1760.8	2043.3	1.8	8.2	22.0
		1×10^{-5}	1729.8	1949.2	1.7	7.6	22.4
2	1:1	1×10^{-2}	2030.0	Superhigh	Superhigh	Superhigh	100.0
		1×10^{-3}	2022.3	2152.1	3.6	17.3	20.8
		1×10^{-4}	1968.3	2106.5	3.8	21.2	17.9
		1×10^{-5}	2006.9	2313.6	17.4	29.3	59.4
	1.5:1	1×10^{-2}	1667.3	2018.0	4.0	14.8	27.0
		1×10^{-3}	1704.6	1986.4	4.4	14.8	29.7
		1×10^{-4}	1930.2	2105.9	3.0	13.1	22.9
		1×10^{-5}	1811.4	2162.1	3.8	12.4	30.6
	2:1	1×10^{-2}	1850.8	2028.2	2.5	13.0	19.2
		1×10^{-3}	1605.5	1912.0	3.3	11.5	28.7
		1×10^{-4}	1752.6	2083.2	5.6	14.8	37.8
		1×10^{-5}	1605.5	1887.3	2.2	9.5	23.2
	2.5:1	1×10^{-2}	1642.0	1904.9	2.1	8.8	23.9
		1×10^{-3}	1535.2	1904.9	3.3	9.6	34.4
		1×10^{-4}	1685.6	1999.1	2.2	10.2	21.6
		1×10^{-5}	1824.0	2149.5	3.1	9.5	32.6

to be continued

Continued

x(Ni)/%	Aspect ratio	Loading rate/s^{-1}	σ_y/MPa	σ_f/MPa	ε_p/%	ε_f/%	($\varepsilon_p/\varepsilon_f$)/%
3	1:1	1×10^{-2}	1784.4	Superhigh	Superhigh	Superhigh	100.0
		1×10^{-3}	1945.9	2298.1	9.7	24.4	39.8
		1×10^{-4}	2091.1	2198.5	2.7	13.5	20.0
		1×10^{-5}	2106.5	2229.4	1.8	16.5	10.9
	1.5:1	1×10^{-2}	1686.1	1943.8	1.6	10.9	14.7
		1×10^{-3}	1604.7	2030.7	3.6	13.1	27.5
		1×10^{-4}	1930.2	2080.6	1.7	9.9	17.2
		1×10^{-5}	1762.6	2033.7	2.0	11.6	17.2
	2:1	1×10^{-2}	1798.7	2049.6	2.8	10.2	27.5
		1×10^{-3}	1767.1	2011.7	1.2	7.5	16.0
		1×10^{-4}	1904.9	2011.7	0.4	7.1	5.6
		1×10^{-5}	1760.8	1999.1	1.2	7.5	16.0
	2.5:1	1×10^{-2}	1832.2	1908.7	0.8	7.2	11.1
		1×10^{-3}	1700.4	1901.7	2.2	8.3	26.5
		1×10^{-4}	1658.0	1901.7	1.4	7.4	18.9
		1×10^{-5}	1511.9	1957.2	2.6	9.4	27.7
4	1:1	1×10^{-2}	1880.1	2072.2	5.3	19.5	27.2
		1×10^{-3}	1925.3	2300.7	11.0	23.7	46.4
		1×10^{-4}	2040.5	2755.3	17.5	30.3	57.8
		1×10^{-5}	1855.9	2440.7	16.3	29.2	55.8
	1.5:1	1×10^{-2}	1824.0	1986.4	1.5	10.7	14.0
		1×10^{-3}	1974.4	2030.7	0.5	9.2	5.4
		1×10^{-4}	1961.8	2149.5	1.0	8.9	11.2
		1×10^{-5}	1706.5	1866.6	2.5	11.2	22.3
	2:1	1×10^{-2}	1874.9	2065.3	1.0	10.0	10.0
		1×10^{-3}	1948.5	2114.1	1.0	8.5	11.8
		1×10^{-4}	1948.5	2095.6	0.8	9.2	8.7
		1×10^{-5}	1960.8	2114.1	0.7	7.5	9.3
	2.5:1	1×10^{-2}	−	1920.2	−	7.7	0
		1×10^{-3}	−	1936.1	−	7.0	0
		1×10^{-4}	1798.5	2013.2	1.0	6.5	15.4
		1×10^{-5}	1838.5	2098.1	1.6	7.8	20.5

XD−3A diffractometer with Cu K_α. Room-temperature uniaxial compression tests were performed on the BMGs with aspect ratios in the range of 1:1−2.5:1 using an Instron 3369 testing machine at loading rates of 1×10^{-5}−1×10^{-2} s^{-1}, respectively. Two polished end surfaces of the samples for the compression tests were parallel to each other and vertical to the symmetry axis. It should be noted that at least three samples for all studied BMGs were examined in order to obtain the reliable results.

3 Results

The results of XRD and DSC indicate that $Cu_{50}Zr_{40}Ti_{10-x}Ni_x$ ($0\le x\le4$, mole fraction, %) alloys are all in amorphous states, as shown in Ref. [10]. Figures 1−8 present typical room-temperature uniaxial compression stress−strain curves of the studied Cu-based BMGs under differerent aspect ratios and loading rates, respectively. The corresponding mechanical properties are carefully examined and listed in Table 1.

3.1 Loading rate effect

Figure 1 presents the room temperature compression stress−strain curves of the studied Cu-based BMGs at different loading rates in condition of an aspect ratio of H/D=1:1. The superplasticity can be clearly

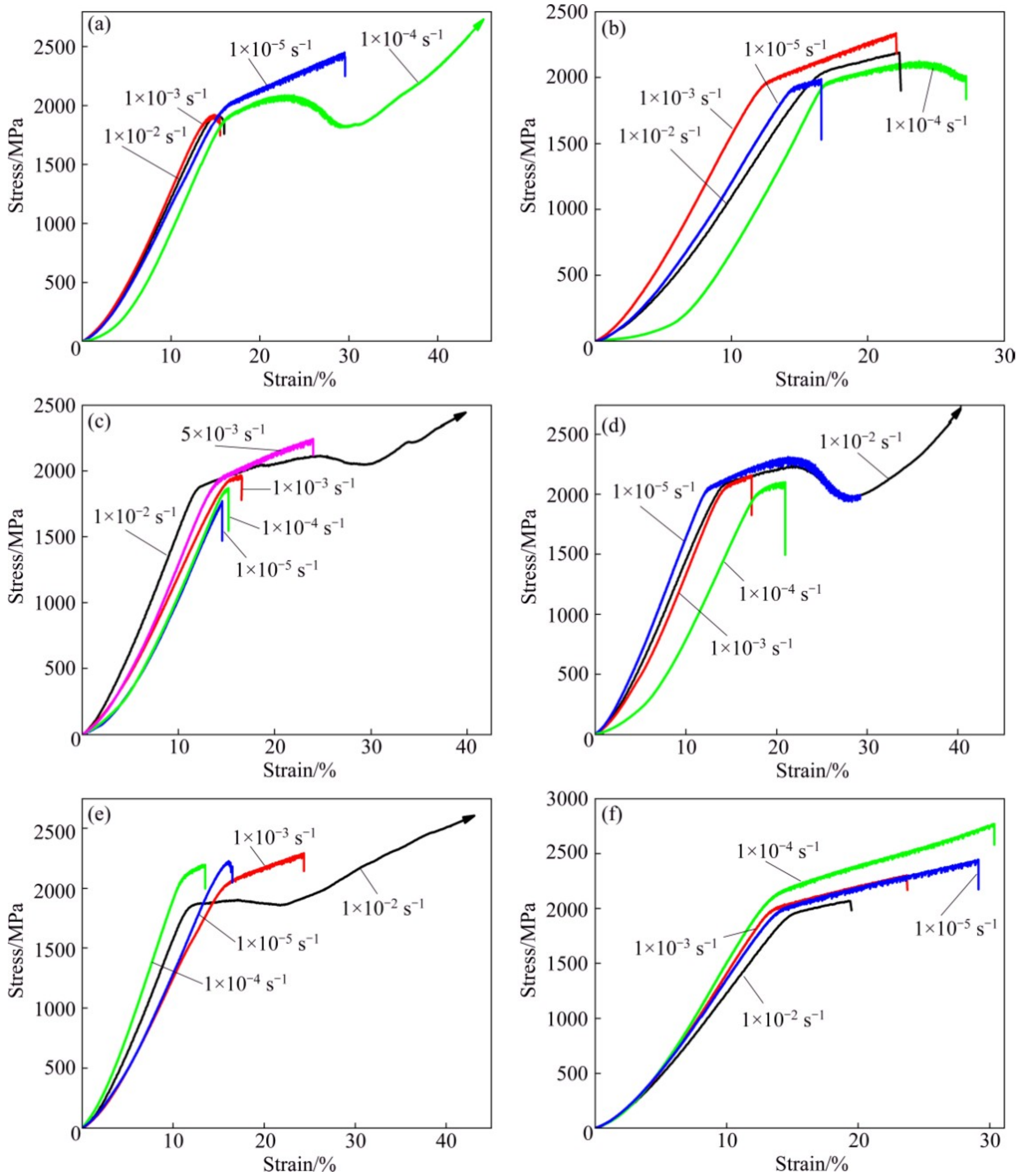

Fig. 1 Room temperature compression stress−strain curves of $Cu_{50}Zr_{40}Ti_{10-x}Ni_x$ ($0\le x\le 4$) BMGs with aspect ratio of 1:1 at different loading rates: (a) x=0; (b) x=0.5; (c) x=1; (d) x=2; (e) x=3; (f) x=4

observed for $Cu_{50}Zr_{40}Ti_{10}$ BMG at a loading rate of 1×10^{-4} s^{-1} (see Fig. 1(a)) and $Cu_{50}Zr_{40}Ti_{10-x}Ni_x$ ($1.0\le x\le 3.0$) BMGs at a loading rate of 1×10^{-2} s^{-1} (see Figs. 1(c)−(e)), while not for the other Cu-based BMGs at the studied loading rates. In addition, there is no plasticity for $Cu_{50}Zr_{40}Ti_9Ni_1$ BMG at a loading rate of 1×10^{-5} s^{-1} (see Fig. 1(c)). As shown in Table 1 and Fig. 1, there are maximum ε_p and $\varepsilon_p/\varepsilon_f$ (ε_f is fracture strain) values for $Cu_{50}Zr_{40}Ti_{10-x}Ni_x$ (x=0 and 4) BMGs at a loading rate of 1×10^{-4} s^{-1} (see Figs. 1(a) and (f)), $Cu_{50}Zr_{40}Ti_{9.5}Ni_{0.5}$ BMG at a loading rate of 1×10^{-3} s^{-1} (see Fig. 1(b)), and $Cu_{50}Zr_{40}Ti_{10-x}Ni_x$ ($1\le x\le 3$) BMGs at a loading rate of 1×10^{-2} s^{-1} (see Figs. 1(c)−(e)), respectively. In addition, the ε_p and $\varepsilon_p/\varepsilon_f$ at high loading rates ($\ge 1\times10^{-3}$ s^{-1}) are smaller than those for low loading rates ($\le 1\times10^{-4}$ s^{-1}) for $Cu_{50}Zr_{40}Ti_{10-x}Ni_x$ (x=0 and 4) BMGs. However, the ε_p and $\varepsilon_p/\varepsilon_f$ at high loading rates ($\ge 1\times10^{-4}$ s^{-1}) are larger than those at low loading rates ($\le 1\times10^{-5}$ s^{-1}) for $Cu_{50}Zr_{40}Ti_{9.5}Ni_{0.5}$ BMG. Interestingly, the ε_p and $\varepsilon_p/\varepsilon_f$ increase with the increase of the loading rate for $Cu_{50}Zr_{40}Ti_{10-x}Ni_x$ (x=1 and 3) BMGs. As for $Cu_{50}Zr_{40}Ti_8Ni_2$ BMG, the ε_p and $\varepsilon_p/\varepsilon_f$ at loading rates of 1×10^{-3} and 1×10^{-4} s^{-1} are smaller than those at loading rates of 1×10^{-2} and 1×10^{-5} s^{-1}. On the other hand, there is a minimum σ_y for $Cu_{50}Zr_{40}Ti_{10-x}Ni_x$ (x=0 and 0.5) BMGs at a loading rate of 1×10^{-3} s^{-1}, $Cu_{50}Zr_{40}Ti_{10-x}Ni_x$ (x=2 and 4) BMGs at a loading rate of 1×10^{-4} s^{-1}, $Cu_{50}Zr_{40}Ti_9Ni_1$ BMG at a loading rate of 1×10^{-4} s^{-1}, respectively. The σ_y of $Cu_{50}Zr_{40}Ti_6Ni_4$ BMG firstly increases with the decrease of the loading rate, and then decreases when the loading rate exceeds 1×10^{-4} s^{-1}. However, the σ_y of $Cu_{50}Zr_{40}Ti_7Ni_3$ BMG increases with the decrease of the loading rate. There is a maximum σ_f for $Cu_{50}Zr_{40}Ti_{10-x}Ni_x$ (x=2 and 3) BMGs at a loading rate of 1×10^{-2} s^{-1}, $Cu_{50}Zr_{40}Ti_{9.5}Ni_{0.5}$ BMG at a loading rate of 1×10^{-3} s^{-1}, and $Cu_{50}Zr_{40}Ti_{10-x}Ni_x$ (x=0 and 4) BMGs at a loading rate of 1×10^{-4} s^{-1}, respectively. As for $Cu_{50}Zr_{40}Ti_{10-x}Ni_x$ (x=0, 0.5 and 4) BMGs, the σ_f firstly increases with the decrease of the loading rate, and then decreases when the loading rate exceeds 1×10^{-4} s^{-1}. However, the σ_f of $Cu_{50}Zr_{40}Ti_9Ni_1$ BMG increases with the decrease of the loading rate.

Figure 2 presents the room temperature compression stress−strain curves of the studied Cu-based BMGs at different loading rates in the condition of an aspect ratio of H/D=1.5:1. All Cu-based BMGs characterize in some plasticity at the studied loading rates except for $Cu_{50}Zr_{40}Ti_9Ni_1$ at a loading rate of 1×10^{-2} s^{-1}. It is found from Fig. 2 and Table 1 that the ε_p and $\varepsilon_p/\varepsilon_f$ of $Cu_{50}Zr_{40}Ti_{10}$ BMG at loading rates of 1×10^{-2}, 1×10^{-4}, and 1×10^{-5} s^{-1} are almost the same and larger than those at the other loading rates. Both ε_p and $\varepsilon_p/\varepsilon_f$ reach up to a maximum value for $Cu_{50}Zr_{40}Ti_{10-x}Ni_x$ (x=1 and 3) BMGs at a loading rate of 1×10^{-3} s^{-1}, $Cu_{50}Zr_{40}Ti_{9.5}Ni_{0.5}$ BMG at a loading rate of 1×10^{-4} s^{-1}, and $Cu_{50}Zr_{40}Ti_{10-x}Ni_x$ (x=0 and 4) BMGs at a loading rate of 1×10^{-5} s^{-1}, respectively. The ε_p and $\varepsilon_p/\varepsilon_f$ of $Cu_{50}Zr_{40}Ti_8Ni_2$ BMG are the largest when the loading rates are 1×10^{-3} and 1×10^{-5} s^{-1}, respectively. In addition, the ε_p and $\varepsilon_p/\varepsilon_f$ firstly decrease with the decrease of

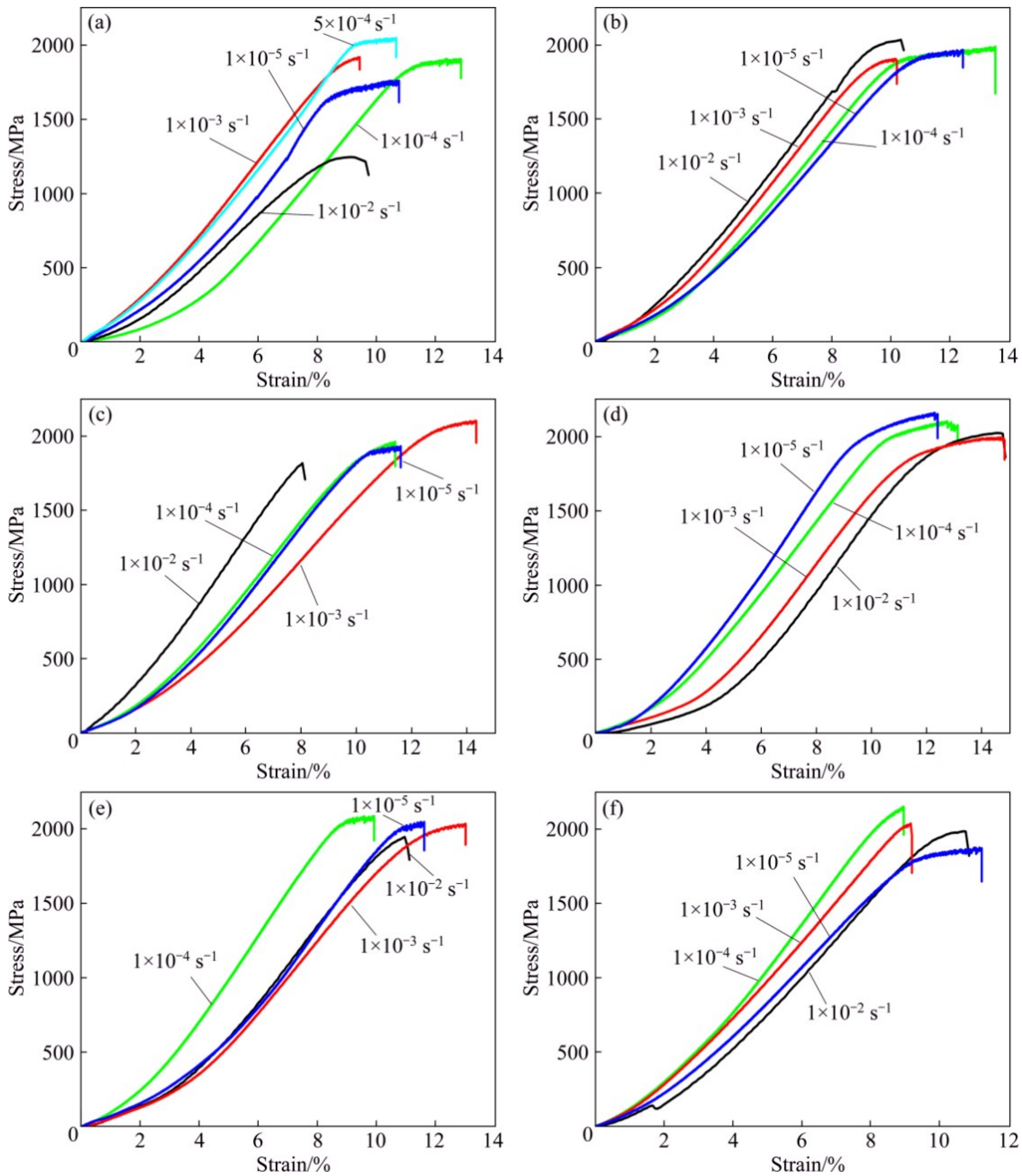

Fig. 2 Room temperature compression stress−strain curves of $Cu_{50}Zr_{40}Ti_{10-x}Ni_x$ ($0\le x\le4$) BMGs with aspect ratio of 1.5:1 at different loading rates: (a) x=0; (b) x=0.5; (c) x=1; (d) x=2; (e) x=3; (f) x=4

the loading rate and then increase when the loading rate exceeds 1×10^{-3} s^{-1} for $Cu_{50}Zr_{40}Ti_{10-x}Ni_x$ (x=0 and 4) BMGs. However, the ε_p and $\varepsilon_p/\varepsilon_f$ firstly increase with the decrease of the loading rate and then decrease when the loading rate exceeds 1×10^{-3} s^{-1} for $Cu_{50}Zr_{40}Ti_9Ni_1$ BMG and 1×10^{-4} s^{-1} for $Cu_{50}Zr_{40}Ti_{9.5}Ni_{0.5}$ BMG. On the other hand, both σ_f and σ_y are the largest for $Cu_{50}Zr_{40}Ti_{10}$ BMG at a loading rate of 5×10^{-4} s^{-1}, $Cu_{50}Zr_{40}Ti_{9.5}Ni_{0.5}$ BMG at a loading rate of 1×10^{-2} s^{-1}, $Cu_{50}Zr_{40}Ti_9Ni_1$ BMG at a loading rate of 1×10^{-3} s^{-1}, and $Cu_{50}Zr_{40}Ti_7Ni_3$ BMG at a loading rate of 1×10^{-4} s^{-1}. The σ_y is the largest for $Cu_{50}Zr_{40}Ti_8Ni_2$ and $Cu_{50}Zr_{40}Ti_6Ni_4$ BMGs when the loading rates are 1×10^{-4} and 1×10^{-3} s^{-1}, respectively. The σ_f is the largest for $Cu_{50}Zr_{40}Ti_8Ni_2$ and $Cu_{50}Zr_{40}Ti_6Ni_4$ BMGs when the loading rates are 1×10^{-5} and 1×10^{-4} s^{-1}, respectively. In addition, the σ_y firstly increases with the decrease of the loading rate and then decreases when the loading rate exceeds 5×10^{-4} s^{-1} for $Cu_{50}Zr_{40}Ti_{10}$ BMG, 1×10^{-4} s^{-1} for $Cu_{50}Zr_{40}Ti_8Ni_2$ BMG, and 1×10^{-3} s^{-1} for $Cu_{50}Zr_{40}Ti_6Ni_4$ BMG, respectively. The σ_f firstly increases with the decrease of the loading rate and then decreases when the loading rate exceeds 5×10^{-4} s^{-1} for $Cu_{50}Zr_{40}Ti_{10}$ BMG, 1×10^{-3} s^{-1} for $Cu_{50}Zr_{40}Ti_9Ni_1$ BMG, and 1×10^{-4} s^{-1} for $Cu_{50}Zr_{40}Ti_6Ni_4$ BMG, respectively. However, the σ_f firstly decreases with the decrease of the loading rate and then increases when the loading rate exceeds 1×10^{-3} s^{-1} for $Cu_{50}Zr_{40}Ti_9Ni_1$ BMG.

Figure 3 presents the room temperature compression stress−strain curves of the studied Cu-based BMGs at different loading rates in the condition of an

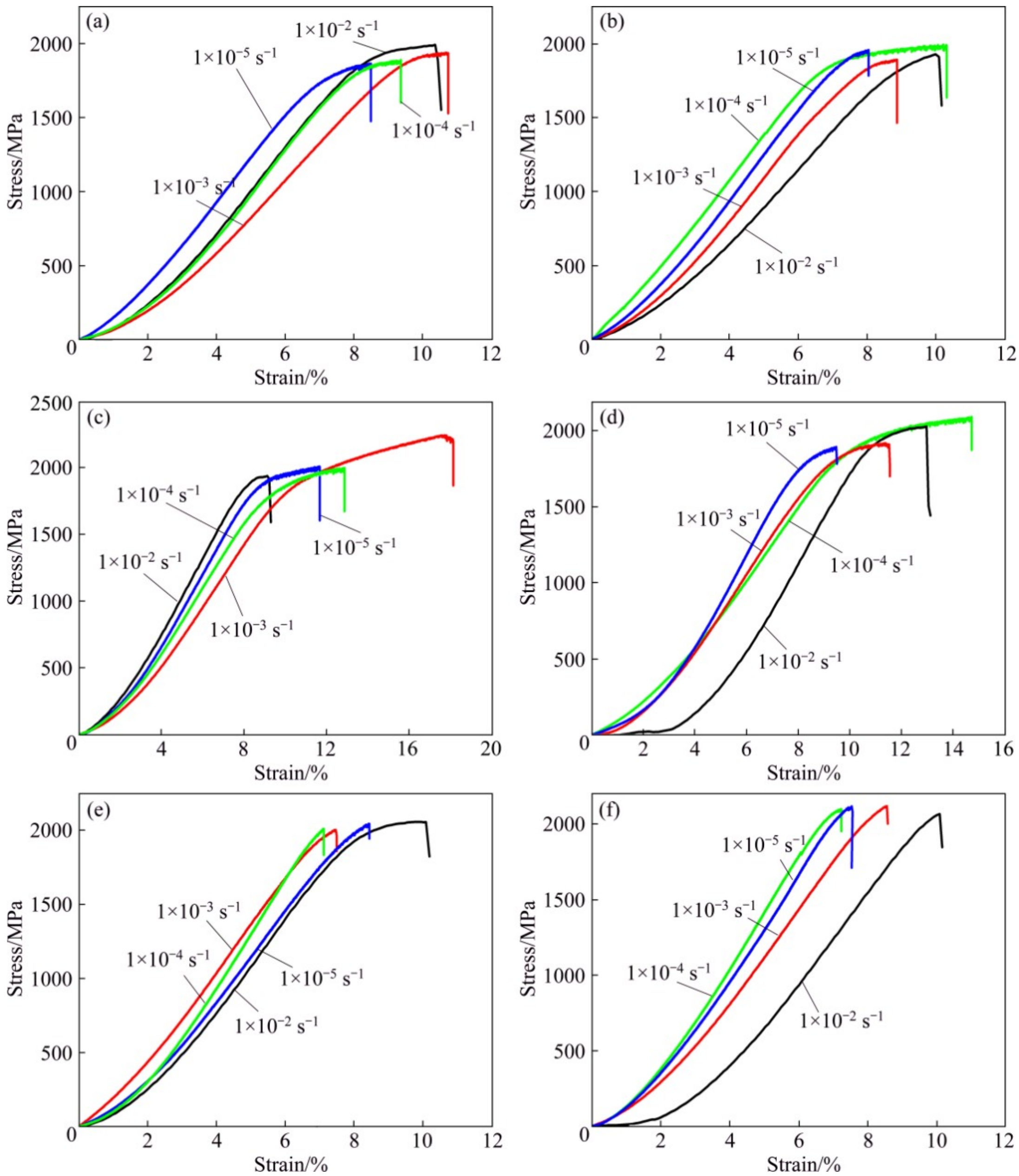

Fig. 3 Room temperature compression stress−strain curves of $Cu_{50}Zr_{40}Ti_{10-x}Ni_x$ ($0\le x\le4$) BMGs with aspect ratio of 2:1 at different loading rates: (a) x=0; (b) x=0.5; (c) x=1; (d) x=2; (e) x=3; (f) x=4

aspect ratio of H/D=2:1. It is found that the Cu-based BMGs all characterize in the plasticity. Both ε_p and $\varepsilon_p/\varepsilon_f$ are the largest for $Cu_{50}Zr_{40}Ti_{10-x}Ni_x$ (x=0 and 3) BMGs at a loading rate of 1×10^{-2} s^{-1}, $Cu_{50}Zr_{40}Ti_{10-x}Ni_x$ (x=1 and 4) BMGs at a loading rate of 1×10^{-3} s^{-1} and $Cu_{50}Zr_{40}Ti_{10-x}Ni_x$ (x=0.5 and 2) BMGs at a loading rate of 1×10^{-4} s^{-1}, respectively. Both ε_p and $\varepsilon_p/\varepsilon_f$ of $Cu_{50}Zr_{40}Ti_{10}$ BMG firstly decrease with the decrease of the loading rate and then increase when the loading rate exceeds 1×10^{-3} s^{-1}. However, both ε_p and $\varepsilon_p/\varepsilon_f$ firstly increase with the decrease of the loading rate and then decrease when the loading rate exceeds 1×10^{-3} s^{-1} for $Cu_{50}Zr_{40}Ti_9Ni_1$ BMG and 1×10^{-4} s^{-1} for $Cu_{50}Zr_{40}Ti_8Ni_2$ BMG. On the other hand, the σ_y is the largest for $Cu_{50}Zr_{40}Ti_{10-x}Ni_x$ (x=1 and 2), $Cu_{50}Zr_{40}Ti_{10}$, $Cu_{50}Zr_{40}Ti_{10-x}Ni_x$ (x=0.5 and 3), and $Cu_{50}Zr_{40}Ti_6Ni_4$ BMGs when the loading rates are 1×10^{-3}, 1×10^{-4}, 1×10^{-2}, and 1×10^{-5} s^{-1}, respectively. The σ_y of $Cu_{50}Zr_{40}Ti_{10}$ BMG firstly increases with the decrease of the loading rate and then decreases when the loading rate exceeds 1×10^{-3} s^{-1}. Nevertheless, the σ_y of $Cu_{50}Zr_{40}Ti_6Ni_4$ BMG increases with the decrease of the loading rate. In addition, the σ_f is the largest for $Cu_{50}Zr_{40}Ti_{10-x}Ni_x$ (x=0 and 3) BMGs at a loading rate of 1×10^{-2} s^{-1}, $Cu_{50}Zr_{40}Ti_9Ni_1$ BMG at a loading rate of 1×10^{-3} s^{-1}, $Cu_{50}Zr_{40}Ti_{10-x}Ni_x$ (x=0.5 and 2) BMGs at a loading rate of 1×10^{-4} s^{-1}, and $Cu_{50}Zr_{40}Ti_6Ni_4$ BMG at the loading rates of 1×10^{-3} and 1×10^{-5} s^{-1}, respectively. The σ_f of $Cu_{50}Zr_{40}Ti_{10}$ BMG firstly decreases with the decease of the loading rate and then increases when the loading rate exceeds 1×10^{-3} s^{-1}.

Figure 4 presents the room temperature compression stress−strain curves of the studied Cu-based

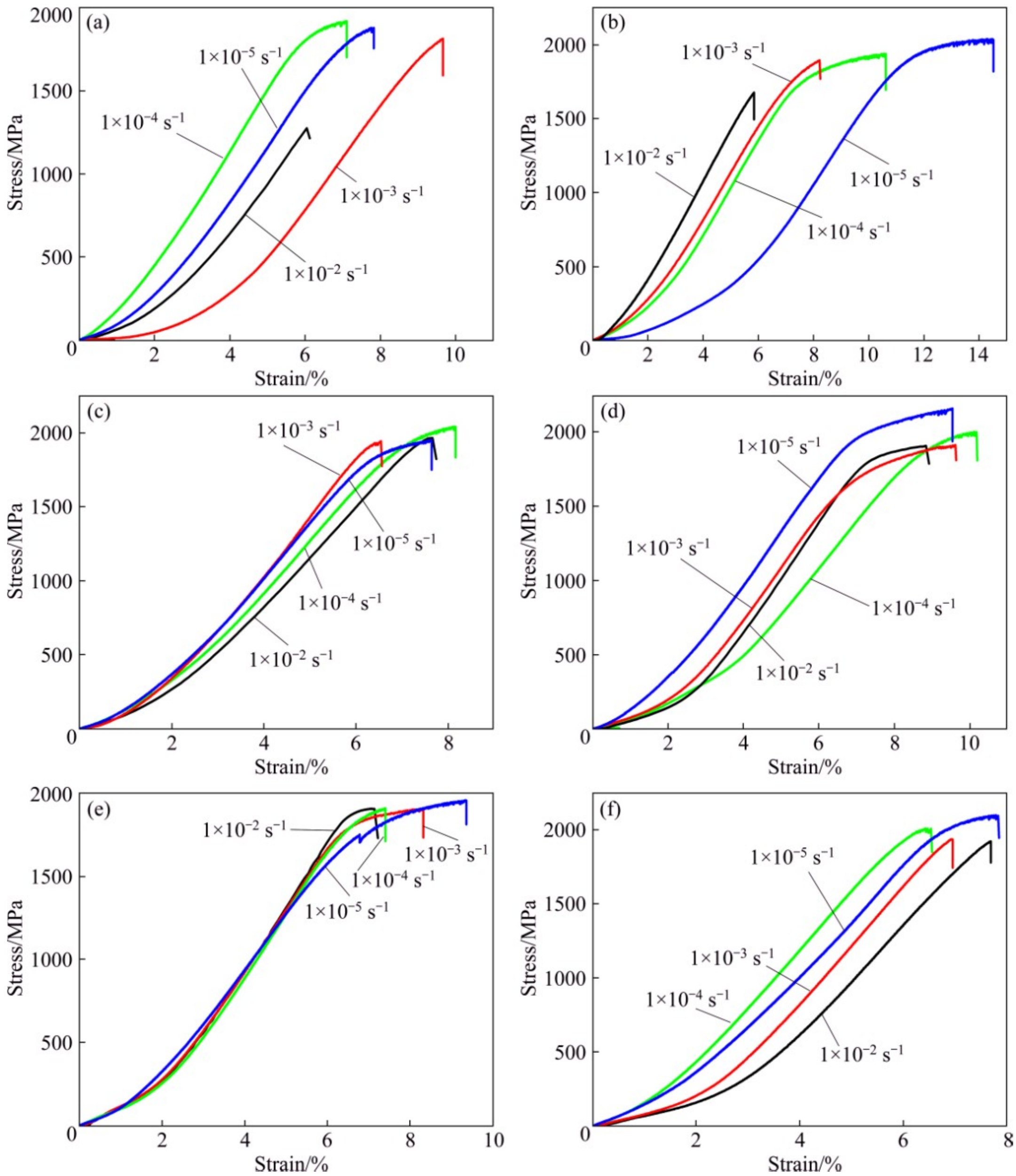

Fig. 4 Room temperature compression stress−strain curves of $Cu_{50}Zr_{40}Ti_{10-x}Ni_x$ ($0\le x\le4$) BMGs with an aspect ratio of 2.5:1 at different loading rates: (a) x=0; (b) x=0.5; (c) x=1; (d) x=2; (e) x=3; (f) x=4

BMGs at different loading rates in the condition of an aspect ratio of *H*/*D*=2.5:1. It is found that the plasticity cannot be observed for $Cu_{50}Zr_{40}Ti_{10-x}Ni_x$ ($0\le x\le 1$) BMGs at a loading rate of 1×10^{-2} s^{-1} and $Cu_{50}Zr_{40}Ti_6Ni_4$ BMG at the loading rates of 1×10^{-2} and 1×10^{-3} s^{-1}. As shown in Table 1, the ε_p of $Cu_{50}Zr_{40}Ti_{10-x}Ni_x$ (x=0.5 and 4) BMGs and the $\varepsilon_p/\varepsilon_f$ of $Cu_{50}Zr_{40}Ti_{10-x}Ni_x$ (x=1 and 4) BMGs increase with the decrease of the loading rate. The ε_p of $Cu_{50}Zr_{40}Ti_{10-x}Ni_x$ (x=0 and 1) BMGs and the $\varepsilon_p/\varepsilon_f$ of $Cu_{50}Zr_{40}Ti_{10-x}Ni_x$ (x=0 and 0.5) BMGs firstly increase with the decrease of the loading rate and then decrease when the loading rate exceeds 1×10^{-4} s^{-1}. The ε_p and $\varepsilon_p/\varepsilon_f$ of $Cu_{50}Zr_{40}Ti_{10-x}Ni_x$ (x=2 and 3) BMGs at the loading rates of 1×10^{-3} and 1×10^{-5} s^{-1} are almost the same and larger than those at the other loading rates. In addition, the σ_y of $Cu_{50}Zr_{40}Ti_{10-x}Ni_x$ (x=0, 0.5 and 4) BMGs and the σ_f of $Cu_{50}Zr_{40}Ti_{10-x}Ni_x$ (x=0.5, 2 and 4) BMGs increase with the decrease of the loading rate, while inversely for $Cu_{50}Zr_{40}Ti_7Ni_3$ BMG. The σ_f of $Cu_{50}Zr_{40}Ti_{10}$ BMG firstly increases with the decrease of the loading rate and then decreases when the loading rate exceeds 1×10^{-4} s^{-1}. However, there is a complex dependence of the σ_y on the loading rate for $Cu_{50}Zr_{40}Ti_{10-x}Ni_x$ (x=1 and 2) BMGs. The σ_y is the largest for $Cu_{50}Zr_{40}Ti_9Ni_1$ and $Cu_{50}Zr_{40}Ti_8Ni_2$ BMGs when the loading rates are 1×10^{-4} and 1×10^{-5} s^{-1}, respectively.

3.2 Aspect ratio effect

Figure 5 presents the room temperature compression stress−strain curves of the studied Cu-based

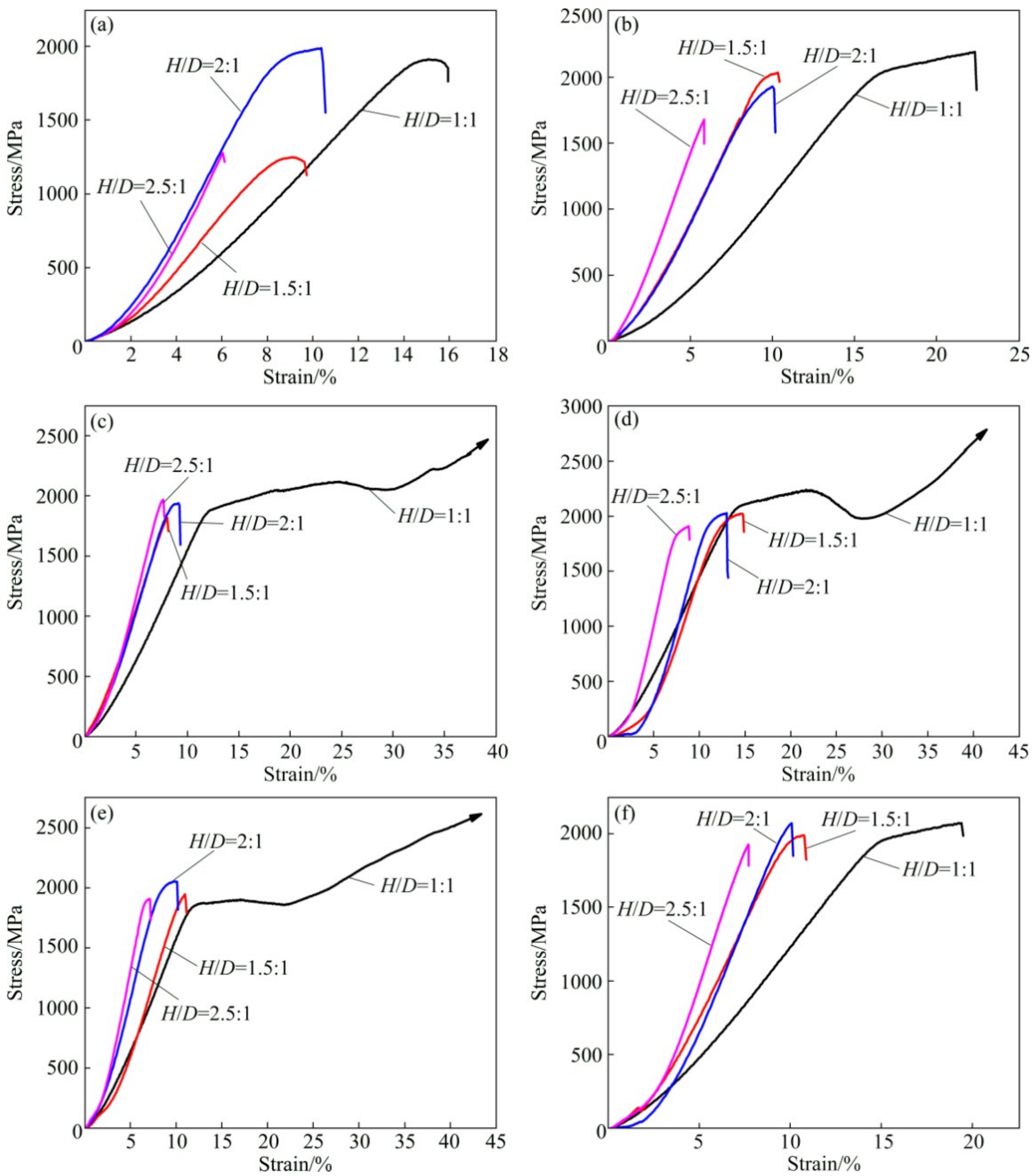

Fig. 5 Room temperature compression stress−strain curves of $Cu_{50}Zr_{40}Ti_{10-x}Ni_x$ ($0\le x\le 4$) BMGs with different aspect ratios at loading rate of 1×10^{-2} s^{-1}: (a) x=0; (b) x=0.5; (c) x=1; (d) x=2; (e) x=3; (f) x=4

BMGs at different aspect ratios under a loading rate of 1×10^{-2} s^{-1}. It is found from Fig. 5 and Table 1 that the plasticity cannot be observed for $Cu_{50}Zr_{40}Ti_{10-x}Ni_x$ (x=0, 0.5 and 4) BMGs with an aspect ratio of 2.5:1 and $Cu_{50}Zr_{40}Ti_7Ni_3$ BMG with an aspect ratio of 1.5:1, while superplasticity is observed for $Cu_{50}Zr_{40}Ti_{10-x}Ni_x$ ($1\le x\le3$) BMGs with an aspect ratio of 1:1. The plasticity of $Cu_{50}Zr_{40}Ti_{10-x}Ni_x$ ($0.5\le x\le4$) BMGs with an aspect ratio of 1:1 is larger than that of the other aspect ratios. Both ε_p and $\varepsilon_p/\varepsilon_f$ of $Cu_{50}Zr_{40}Ti_{10}$ BMG firstly increase and then decrease down to zero when the aspect ratio increases up to 2.5:1. The ε_p decreases with increasing aspect ratio for $Cu_{50}Zr_{40}Ti_{10-x}Ni_x$ (x=2 and 4) BMGs. In addition, both σ_y and σ_f of $Cu_{50}Zr_{40}Ti_{9.5}Ni_{0.5}$ BMG decrease with increasing aspect ratio. The σ_f of $Cu_{50}Zr_{40}Ti_8Ni_2$ BMG almost decreases with increasing aspect ratio. The σ_f of $Cu_{50}Zr_{40}Ti_9Ni_1$ BMG firstly decreases with increasing aspect ratio and then increases when the aspect ratio exceeds 1.5:1. However, there are complex dependences of the aspect ratio for the σ_y of $Cu_{50}Zr_{40}Ti_{10-x}Ni_x$ (x=0 and $1\le x\le4$) BMGs and the σ_f of $Cu_{50}Zr_{40}Ti_{10-x}Ni_x$ (x=0, 3 and 4) BMGs. Both σ_y and σ_f of $Cu_{50}Zr_{40}Ti_{10-x}Ni_x$ (x=0 and 2) BMGs with the aspect ratios of 1:1 and 2:1 are larger than those with the aspect ratios of 1.5:1 and 2.5:1. The σ_y is the largest for $Cu_{50}Zr_{40}Ti_{10-x}Ni_x$ (x=0, 2 and 4) and $Cu_{50}Zr_{40}Ti_{10-x}Ni_x$ (x=1 and 3) BMGs when the aspect ratios are 1:1 and 2.5:1, respectively. The σ_f is the largest for $Cu_{50}Zr_{40}Ti_{10}$ and $Cu_{50}Zr_{40}Ti_{10-x}Ni_x$ (x=3 and 4) BMGs when the aspect ratios are 2:1 and 1:1, respectively. More interestingly, the σ_y of $Cu_{50}Zr_{40}Ti_{10-x}Ni_x$ ($1\le x\le4$) BMGs with an aspect ratio of 1:1 is close to the σ_f with the other aspect ratios.

Figure 6 presents the room temperature compression stress−strain curves of the studied Cu-based

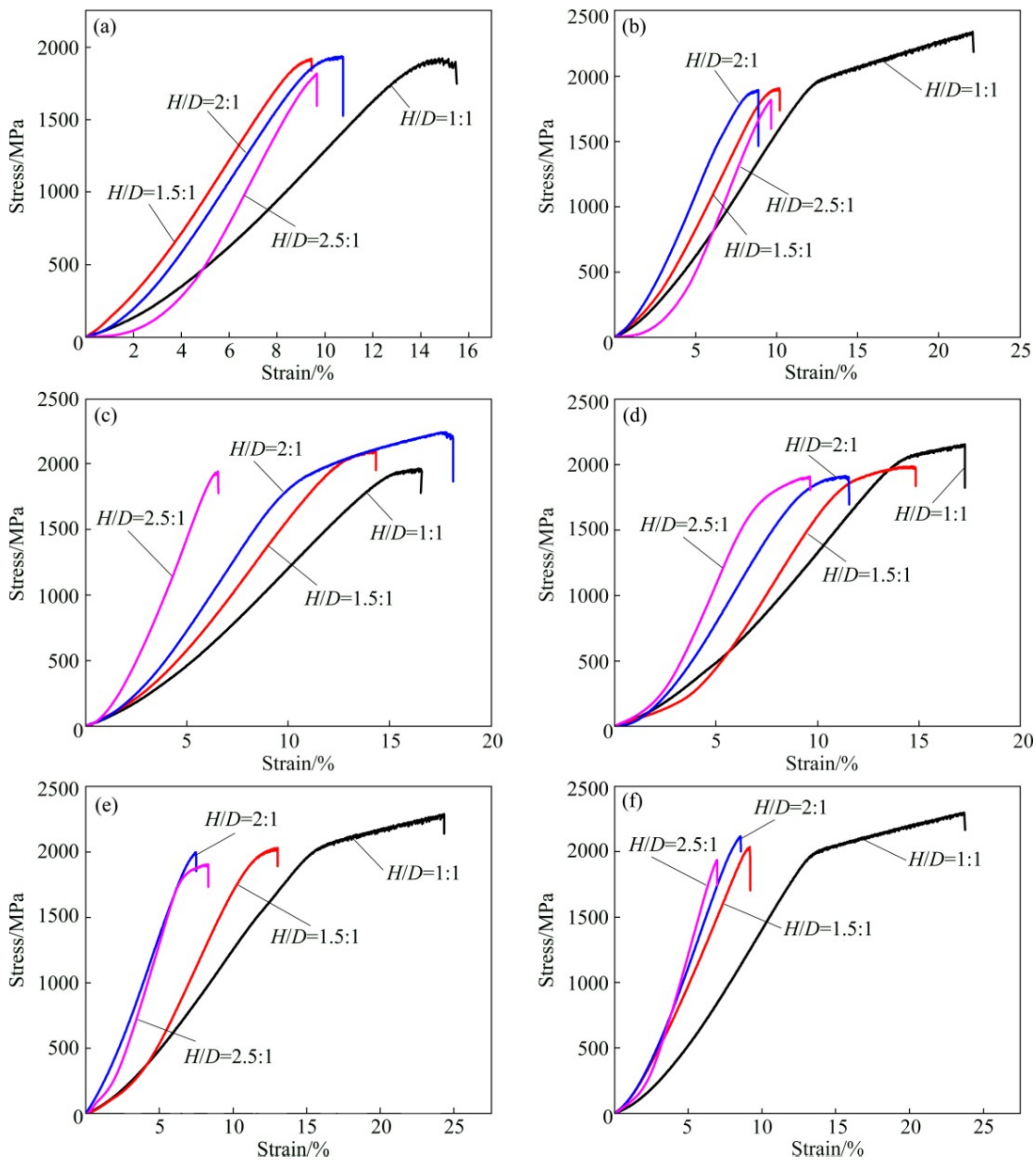

Fig. 6 Room temperature compression stress−strain curves of $Cu_{50}Zr_{40}Ti_{10-x}Ni_x$ ($0\le x\le4$) BMGs with different aspect ratios at loading rate of 1×10^{-3} s^{-1}: (a) x=0; (b) x=0.5; (c) x=1; (d) x=2; (e) x=3; (f) x=4

BMGs at different aspect ratios under a loading rate of 1×10^{-3} s^{-1}. As shown in Fig. 6 and Table 1, the ε_p firstly increases with increasing aspect ratio and then decreases for $Cu_{50}Zr_{40}Ti_8Ni_2$ BMG when the aspect ratio exceeds 1.5:1. The ε_p decreases with increasing aspect ratio for $Cu_{50}Zr_{40}Ti_7Ni_3$ BMG. However, there is a complex dependence of the ε_p on the aspect ratio for the other Cu-based BMGs. The ε_p is the largest for these Cu-based BMGs with an aspect ratio of 1:1. The ε_p is zero for $Cu_{50}Zr_{40}Ti_6Ni_4$ BMG with an aspect ratio of 2.5:1. The $\varepsilon_p/\varepsilon_f$ firstly decreases with increasing aspect ratio and then increases for $Cu_{50}Zr_{40}Ti_{9.5}Ni_{0.5}$ BMG when the aspect ratio exceeds 1.5:1. The $\varepsilon_p/\varepsilon_f$ is biggest for $Cu_{50}Zr_{40}Ti_{10-x}Ni_x$ (x=0.5, 3 and 4) BMGs with an aspect ratio of 1:1, $Cu_{50}Zr_{40}Ti_{10-x}Ni_x$ (x=0 and 1) BMGs with an aspect ratio of 2:1, and $Cu_{50}Zr_{40}Ti_8Ni_2$ BMG with an aspect ratio of 2.5:1, respectively. In addition, the σ_y decreases with increasing aspect ratio for $Cu_{50}Zr_{40}Ti_{10-x}Ni_x$ (x=0.5 and 2) BMGs. As for $Cu_{50}Zr_{40}Ti_{10-x}Ni_x$ (x=0 and 4) BMGs, the σ_y firstly increases with increasing aspect ratio and then decreases when the aspect ratio exceeds 1.5:1. However, the σ_y firstly decreases with increasing aspect ratio and then increases when the aspect ratio exceeds 2:1. The σ_f decreases with increasing aspect ratio for $Cu_{50}Zr_{40}Ti_{10-x}Ni_x$ (x=0.5, 2 and 3) BMGs. The σ_f of $Cu_{50}Zr_{40}Ti_9Ni_1$ BMG firstly increases with increasing aspect ratio and then decreases when the aspect ratio exceeds 2:1. The σ_f of $Cu_{50}Zr_{40}Ti_{10}$ BMG with the aspect ratio of 1:1−2:1 is almost the same and larger than that with an aspect ratio of 2.5:1. There is a complex dependence of the σ_y for $Cu_{50}Zr_{40}Ti_7Ni_3$ BMG and the σ_f for $Cu_{50}Zr_{40}Ti_6Ni_4$ BMG on the aspect ratio, but the σ_y is the largest for $Cu_{50}Zr_{40}Ti_7Ni_3$ BMG and σ_f is the largest for $Cu_{50}Zr_{40}Ti_6Ni_4$ BMG when the aspect ratio is 1:1. More interestingly, the σ_f of the studied Cu-based BMGs in the range of the aspect ratio of 1.5:1−2.5:1 is close to the σ_y with an aspect ratio of 1:1 except for $Cu_{50}Zr_{40}Ti_9Ni_1$ BMG.

Figure 7 presents the room temperature compression stress−strain curves of the studied Cu-based BMGs at different aspect ratios under a loading rate of 1×10^{-4} s^{-1}. As shown in Fig. 7 and Table 1, $Cu_{50}Zr_{40}Ti_{10}$ BMG with an aspect ratio of 1:1 characterizes in superplasticity. One can also observe some plastic strain for $Cu_{50}Zr_{40}Ti_{10}$ BMG with the aspect ratios of 1.5:1−2.5:1 and $Cu_{50}Zr_{40}Ti_{10-x}Ni_x$ ($0\le x\le4$) BMGs with the aspect ratios of 1:1−2.5:1. The ε_p decreases with increasing aspect ratio for $Cu_{50}Zr_{40}Ti_{10}$ BMG. The ε_p firstly increases with increasing aspect ratio and then decreases when the aspect ratio exceeds 2:1 for $Cu_{50}Zr_{40}Ti_9Ni_1$ BMG, while inversely for $Cu_{50}Zr_{40}Ti_7Ni_3$ BMG. As for $Cu_{50}Zr_{40}Ti_{10-x}Ni_x$ (x=0 and 4) BMGs, the ε_p at the aspect ratios of 1.5:1−2.5:1 is almost same and smaller than that at the aspect ratio of 1:1. The $\varepsilon_p/\varepsilon_f$ firstly increases with increasing aspect ratio and then decreases when the aspect ratio exceeds 2:1 for $Cu_{50}Zr_{40}Ti_{10-x}Ni_x$ (x=1 and 2) BMGs, while inversely for $Cu_{50}Zr_{40}Ti_{10-x}Ni_x$ (x=3 and 4) BMGs. The ε_p is the largest for $Cu_{50}Zr_{40}Ti_8Ni_2$ BMG with an aspect ratio of 2:1. The $\varepsilon_p/\varepsilon_f$ is the largest for $Cu_{50}Zr_{40}Ti_{9.5}Ni_{0.5}$ BMG with an aspect ratio of 2:1 and $Cu_{50}Zr_{40}Ti_{10}$ BMG with an aspect ratio of 1:1. Both σ_y and σ_f decrease with increasing aspect ratio for $Cu_{50}Zr_{40}Ti_{10-x}Ni_x$ (x=2−4) BMGs. The σ_y of $Cu_{50}Zr_{40}Ti_{10-x}Ni_x$ (x=0 and 1) BMGs and the σ_f of $Cu_{50}Zr_{40}Ti_{10}$ BMG firstly decrease with increasing aspect ratio and then increase when the aspect ratio exceeds 2:1. The σ_y of $Cu_{50}Zr_{40}Ti_{9.5}Ni_{0.5}$ BMG decreases with increasing aspect ratio, while inversely for the σ_f of $Cu_{50}Zr_{40}Ti_9Ni_1$ BMG. More interestingly, the σ_f of the studied Cu-based BMGs with the aspect ratios of 1.5:1−2.5:1 is close to the σ_y of that with the aspect ratio of 1:1 except for $Cu_{50}Zr_{40}Ti_9Ni_1$ BMG.

Figure 8 presents the room temperature compression stress−strain curves of the studied Cu-based BMGs at different aspect ratios at a loading rate of 1×10^{-5} s^{-1}. As shown in Fig. 8 and Table 1, all Cu-based BMGs characterize in the plasticity except for $Cu_{50}Zr_{40}Ti_9Ni_1$ BMG with an aspect ratio of 1:1. The ε_p decreases with increasing aspect ratio for $Cu_{50}Zr_{40}Ti_{10}$ BMG. Both ε_p and $\varepsilon_p/\varepsilon_f$ firstly decrease with increasing aspect ratio and then increase when the aspect ratio exceeds 2:1 for $Cu_{50}Zr_{40}Ti_{10-x}Ni_x$ (x=2 and 4) BMGs, while inversely for $Cu_{50}Zr_{40}Ti_9Ni_1$ BMG. There are maximum values for the ε_p and the $\varepsilon_p/\varepsilon_f$ of $Cu_{50}Zr_{40}Ti_{10-x}Ni_x$ (x=0.5 and 3) BMGs with an aspect ratio of 2.5:1. However, the $\varepsilon_p/\varepsilon_f$ is the largest for $Cu_{50}Zr_{40}Ti_{10}$ BMG with an aspect ratio of 1:1. On the other hand, both σ_y and σ_f decrease with increasing aspect ratio for $Cu_{50}Zr_{40}Ti_7Ni_3$ BMG. The σ_y of $Cu_{50}Zr_{40}Ti_{10-x}Ni_x$ (x=0, 0.5 and 2) BMGs and the σ_f of $Cu_{50}Zr_{40}Ti_{10-x}Ni_x$ (x=0.5 and 2) BMGs firstly decrease with increasing aspect ratio and then increase when the aspect ratio exceeds 2:1, while inversely for the σ_f of $Cu_{50}Zr_{40}Ti_9Ni_1$ BMG. The σ_y of $Cu_{50}Zr_{40}Ti_9Ni_1$ BMG firstly increases with increasing aspect ratio and then decreases when the aspect ratio exceeds 1.5:1, while inversely for the σ_f of $Cu_{50}Zr_{40}Ti_{10}$ BMG. The dependence of the σ_y and σ_f on the aspect ratio is complex for $Cu_{50}Zr_{40}Ti_6Ni_4$ BMG. There is a maximum σ_y at the aspect ratio of 2:1 and σ_f at the aspect ratio of 1:1, respectively. Interestingly, the σ_y at the aspect ratio of 1:1 is larger than the σ_f at the aspect ratios of 1.5:1−2.5:1 for $Cu_{50}Zr_{40}Ti_{10}$ and $Cu_{50}Zr_{40}Ti_7Ni_3$ BMGs.

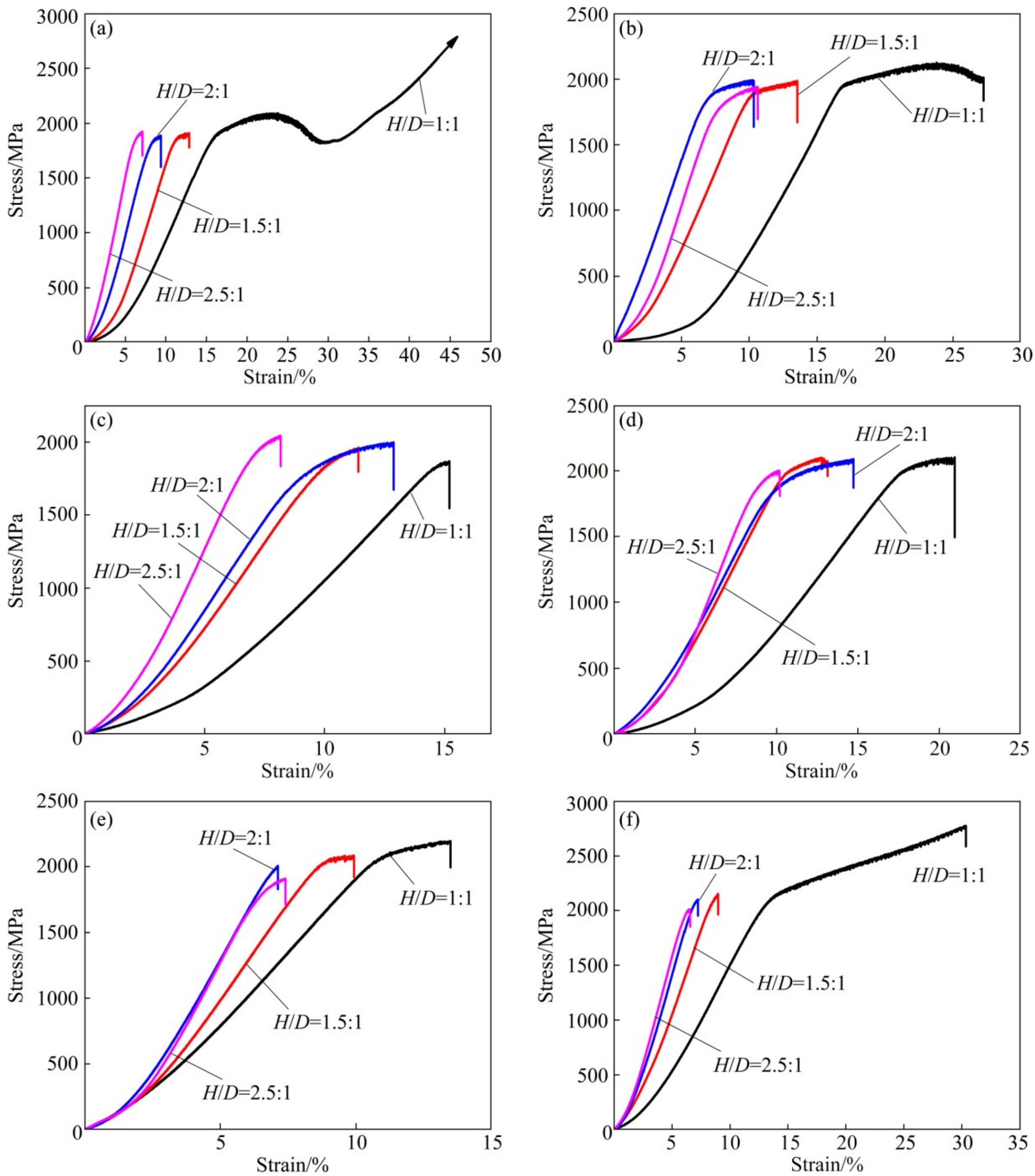

Fig. 7 Room temperature compression stress−strain curves of $Cu_{50}Zr_{40}Ti_{10-x}Ni_x$ ($0 \le x \le 4$) BMGs with different aspect ratios at loading rate of 1×10^{-4} s^{-1}: (a) x=0; (b) x=0.5; (c) x=1; (d) x=2; (e) x=3; (f) x=4

4 Discussion

As shown in Figs. 1−8 and Table 1, the strength and the plasticity of the studied Cu-based BMGs significantly depend on the aspect ratio and the loading rate. For example, the strength of $Cu_{50}Zr_{40}Ti_{10}$ BMG with an aspect ratio of 1.5:1 and the plasticity of $Cu_{50}Zr_{40}Ti_8Ni_2$ BMG with an aspect ratio of 2:1 increase with increasing the loading rate and then decrease when the loading rate reaches up to a critical value. It was also found in $Zr_{56}Al_{10.9}Ni_{4.6}Cu_{27.8}Nb_{0.7}$ BMG [24] and SrCaYbMg(Li)Zn(Cu) BMGs [25], respectively. The yield strength for $Cu_{50}Zr_{40}Ti_9Ni_1$ BMG with an aspect ratio of 1:1 at loading rates from 1×10^{-2} to 1×10^{-4} s^{-1} and the plasticity for $Cu_{50}Zr_{40}Ti_6Ni_4$ BMG with an aspect ratio of 2:1 at loading rates from 1×10^{-2} to 1×10^{-5} s^{-1} almost maintain a constant value, which is similar to the results in Refs. [30−32]. Both strength and strain decrease with increasing the loading rate for $Cu_{50}Zr_{40}Ti_{10}$

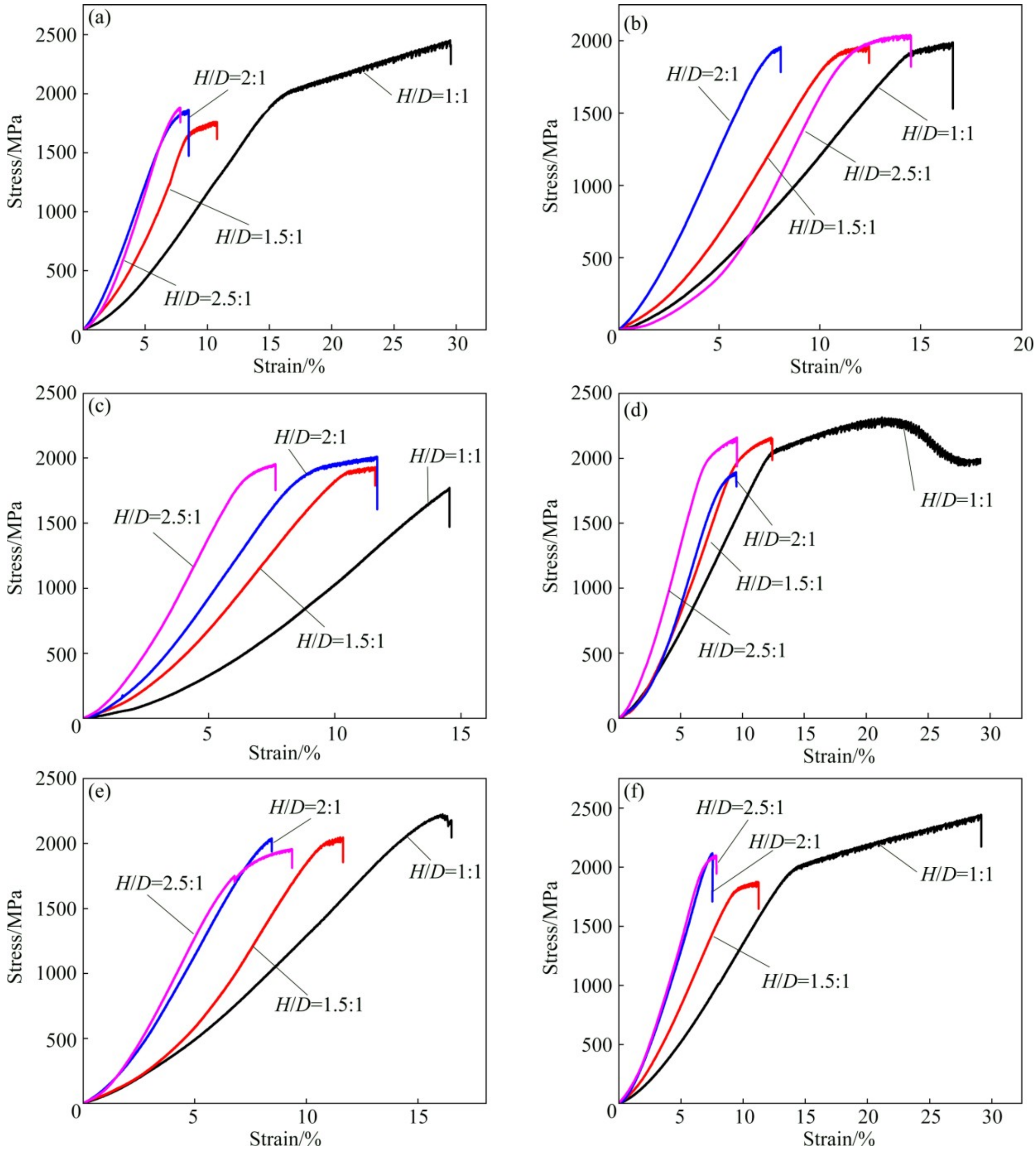

Fig. 8 Room temperature compression stress−strain curves of $Cu_{50}Zr_{40}Ti_{10-x}Ni_x$ ($0 \le x \le 4$) BMGs with different aspect ratios at loading rate of 1×10^{-5} s^{-1}: (a) x=0; (b) x=0.5; (c) x=1; (d) x=2; (e) x=3; (f) x=4

BMG with an aspect ratio of 2.5:1, which is similar to the results in Refs. [20,26−29,31]. However, the yield strength for $Cu_{50}Zr_{40}Ti_7Ni_3$ BMG with an aspect ratio of 2.5:1 and the strain for $Cu_{50}Zr_{40}Ti_9Ni_1$ BMG with an aspect ratio of 1:1 increase with increasing the loading rate, which was also found in Ti-based BMG [20], Nd-based BMG [27], and Zr-based BMG [33], respectively. Interestingly, in the condition of an aspect ratio of 2:1, the yield strength for $Cu_{50}Zr_{40}Ti_9Ni_1$ BMG and the plastic strain for $Cu_{50}Zr_{40}Ti_7Ni_3$ BMG decrease with increasing the loading rate and then decrease when the aspect ratio reaches up to a critical value, which is not reported in other BMGs up to date. On the other hand, the dependence of the strength and/or the plasticity on the aspect ratio and/or the loading rate varies with the alloy composition for the studied Cu-based BMGs. For instance, when the aspect ratio is 2:1, the yield strength firstly increases with decreasing the loading rate and then decreases for $Cu_{50}Zr_{40}Ti_{10}$ and $Cu_{50}Zr_{40}Ti_{9.5}Ni_{0.5}$ BMGs, while inversely for $Cu_{50}Zr_{40}Ti_9Ni_1$ and $Cu_{50}Zr_{40}Ti_6Ni_4$ BMGs. The plastic strain firstly decreases with decreasing the loading rate and then increases for $Cu_{50}Zr_{40}Ti_{10}$ and $Cu_{50}Zr_{40}Ti_7Ni_3$ BMGs, while inversely for $Cu_{50}Zr_{40}Ti_9Ni_1$ and $Cu_{50}Zr_{40}Ti_8Ni_2$ BMGs. Moreover, the superplasticity can be observed for $Cu_{50}Zr_{40}Ti_{10}$ at a loading rate of 1×10^{-4} s^{-1} and $Cu_{50}Zr_{40}Ti_{10-x}Ni_x$ (x=1−3) BMGs at a loading rate of 1×10^{-2} s^{-1} when the aspect ratio is 1:1. Different mechanical properties of the studied Cu-based BMGs would be resulted from the following factors. Firstly, it is well-known that there are atomic- and/or nano-, even micro-scale microstructures in the BMG [15,41−44]. Compositional difference, even minor addition/substitution would vary the magnitude, type and distribution of these microstructures, which influences the relaxation, diffusion and rearrangement of atoms, resulting in the change of the properties of glass forming alloys [10,43−47]. For example, the superplasticity of Zr-based BMGs developed by LIU et al [15] resulted from the nano-scale microstructure. Different properties of the studied Cu-based BMGs developed by CAI et al [10] would be due to different category, magnitude and distribution of the atomic-scale microstructures. Secondly, the strength and the plasticity of the BMG depend on the emission/propagation rate of the shear bands during deformation. If the emission/propagation rate of the shear bands is consistent with the applied strain rates, shear bands will nucleate and propagate continuously during deformation, resulting in an enhanced strength and plasticity. Obviously, there is a critical loading rate suitable for the emission/propagation rate of the shear bands. SONG et al [24] investigated the effect of strain rate on the compressive behavior of $Zr_{56}Al_{10.9}Ni_{4.6}Cu_{27.8}Nb_{0.7}$ BMG and found that both strength and plasticity increase with increasing the strain rate up to 1×10^{-5} s^{-1}, above which the strength and plasticity start to decrease. Similar results were also found in other BMGs [25]. In addition, the metallic glasses with different compositions were found to display different mechanical response to the loading rate [20,24−33]. Thirdly, the larger the aspect ratio under the same sample size is, the more the atomic, even nano/micro-scale microstructures in the metallic glass are. The shear band generally nucleates at weak sites. Small aspect ratio of the BMG would result in few shear bands due to few weak sites. However, the aspect ratio would result in the confining effect of the compressive sample [21]. The smaller the aspect ratio is, the stronger the confining effect is. It would result in the formation of multiple shear bands in the condition of small aspect ratio [21]. Finally, the plastic flow can be considered as the transition of the metallic glass to the supercooled liquid under external temperature or stress [48]. The external stress would lead to the increase of the temperature [48−50] and free volume [3−7]. The temperature and free volume increase would result in the increase of the atomic mobility and the decrease of the bonding strength among the atoms. The shear band velocity increases with increasing temperature [51]. In addition, CAI et al [6,7] found that the structural and thermal sensitivity of Cu−Zr−Ti metallic glasses to pressure/tension was related to the composition of the metallic glass. Therefore, different mechanical responses of the studied Cu-based BMGs to the loading rate and aspect ratio would be a comprehensive externalization of above-mentioned factors.

5 Conclusions

1) The superplasticity can be clearly observed for $Cu_{50}Zr_{40}Ti_{10}$ BMG with an aspect ratio of 1:1 at a loading rate of 1×10^{-4} s^{-1} and $Cu_{50}Zr_{40}Ti_{10-x}Ni_x$ (x=1−3) BMGs with an aspect ratio of 1:1 at a loading rate of 1×10^{-2} s^{-1}, while no plasticity for $Cu_{50}Zr_{40}Ti_{10-x}Ni_x$ (x=0, 0.5 and 4) BMGs with an aspect ratio of 2.5:1 at a loading rate of 1×10^{-2} s^{-1}, $Cu_{50}Zr_{40}Ti_6Ni_4$ BMG with an aspect ratio of 2.5:1 at a loading rate of 1×10^{-3} s^{-1}, $Cu_{50}Zr_{40}Ti_9Ni_1$ BMG with an aspect ratio of 1:1 at a loading rate of 1×10^{-5} s^{-1}, respectively.

2) There are complex relationships between the mechanical properties and the aspect ratio and the loading rate for the studied Cu-based BMGs, which depend on the content of Ni, the aspect ratio, and the loading rate. The largest yielding strength σ_y can be up to 2106.5 MPa for $Cu_{50}Zr_{40}Ti_9Ni_1$ BMG with an aspect ratio of 1:1 at a loading rate of 1×10^{-5} s^{-1}.

3) The σ_y at an aspect ratio of 1:1 is close to the σ_f of the other aspect ratios for $Cu_{50}Zr_{40}Ti_{10-x}Ni_x$ ($1\le x\le4$) BMGs at a loading rate of 1×10^{-2} s^{-1}. The σ_f at the aspect ratios of 1.5:1−2.5:1 is close to the σ_y at an aspect ratio of 1:1 for all studied Cu-based BMG except for $Cu_{50}Zr_{40}Ti_9Ni_1$ BMG at loading rates of 1×10^{-3} and 1×10^{-4} s^{-1}. The σ_y at an aspect ratio of 1:1 is larger than the σ_f at the aspect ratios of 1.5:1−2.5:1 of $Cu_{50}Zr_{40}Ti_{10}$ and $Cu_{50}Zr_{40}Ti_7Ni_3$ BMGs at a loading rate of 1×10^{-5} s^{-1}.

References

[1] PAN Y, CAO H B, DING L, ZHANG C, CHANG Y A. Novel bulkier copper-rich ternary metallic glasses from computational thermodynamics [J]. Journal of Non-Crystalline Solids, 2010, 356: 2168−2171.

[2] PAN Y, ZENG Y Q, JING L J, ZHANG L, PI J H. Composition design and mechanical properties of ternary Cu−Zr−Ti bulk metallic glasses [J]. Materials & Design, 2014, 55: 773−777.

[3] AN W K, CAI A H, XIONG X, LIU Y, ZHOU G J, LUO Y, LI T L, LI X S. Effect of tension on corrosive and thermal properties of $Cu_{60}Zr_{30}Ti_{10}$ metallic glass [J]. Journal of Alloys and Compounds, 2013, 563: 55−62.

[4] AN W K, CAI A H, XIONG X, LIU Y, ZHOU G J, LUO Y, LI T L, LI X S. Tensile effect on corrosive and thermal properties of $Cu_{55}Zr_{35}Ti_{10}$ metallic glass [J]. Materials Science and Engineering A, 2013, 564: 442−449.

[5] CAI A H, DING D W, XIONG X, LIU Y, AN W K, ZHOU G J, LUO Y, LI T L, WANG H, WU Y. Effect of mechanical tension on

corrosive and thermal properties of $Cu_{50}Zr_{40}Ti_{10}$ metallic glass [J]. Materials Science and Engineering A, 2013, 588: 49−58.

[6] CAI A H, XIONG X, LIU Y, AN W K, ZHOU G J, LUO Y, LI T L, LI X S. Structural and thermal sensitivity of Cu−Zr−Ti amorphous alloys to pressure [J]. Journal of Non-Crystalline Solids, 2013, 379: 1−6.

[7] CAI An-hui, XIONG Xiang, LIU Yong, AN Wei-ke, ZHOU Guo-jun, LUO Yun, LI Tie-lin, LI Xiao-song. Structural and thermal sensitivity of Cu−Zr−Ti amorphous alloys to tension [J]. Science China: Physics, Mechanics & Astronomy, 2013, 56: 1606−1610.

[8] CAI An-hui, AN Wei-ke, LI Xiao-song, LUO Yun, LI Tie-lin. Property of Cu−Zr−Ti ternary alloys [J]. Advanced Materials Research, 2011, 146–147: 1477−1481.

[9] LU Z P, BEI H, LIU C T. Recent progress in quantifying glass-forming ability of bulk metallic glasses [J]. Intermetallics, 2007, 15: 618−624.

[10] CAI A H, DING D W, AN W K, ZHOU G J, LUO Y, LI J H, PENG Y Y. Effect of Ni substitution on glass forming ability, mechanical, electrical and thermal properties of Cu−Zr−Ti glass forming alloys [J]. Materials Chemistry and Physics, 2015, 151: 243−251.

[11] WU Ji-li, PAN Ye, LI Xing-zhou, WANG Xian-fei. Designing plastic Cu-based bulk metallic glass via minor addition of nickel [J]. Materials & Design, 2014, 57: 175−179.

[12] WU Ji-li, PAN Ye, LI Xing-zhou, WANG Xian-fei. Composition design of plastic Cu−Zr−Ti−Ni bulk metallic glass: A liquidus perspective [J]. Materials Science and Engineering A, 2014, 608: 16−20.

[13] ZHANG T, MEN H, PANG S J, FU J Y, MA C L, INOUE A. Effects of a minor addition of Si and/or Sn on formation and mechanical properties of Cu−Zr−Ti bulk metallic glass [J]. Materials Science and Engineering A, 2007, 449−451: 295−298.

[14] WU Ji-li, PAN Ye, LI Xing-zhou, WANG Xian-fei. Microstructure evolution and mechanical properties of Nb-alloyed Cu-based bulk metallic glasses and composites [J]. Materials & Design, 2015, 75: 32−39.

[15] LIU Y H, WANG G, WANG R J, ZHAO D Q, PAN M X, WANG W H. Super plastic bulk metallic glasses at room temperature [J]. Science, 2007, 315: 1385−1388.

[16] CAI An-hui, LIU Yong, WU Hong, DING Da-wei, AN Wei-ke, ZHOU Guo-jun, LUO Yun, PENG Yong-yi. Phase formation, glass forming ability, mechanical and thermal properties of $Cu_{50}Zr_{50-x}Al_x$ ($0\leq x\leq 11.0$) glass forming alloys [J]. Science China: Materials, 2015, 58: 584−594.

[17] SAEIDABADI E K, GHOLAMIPOUR R, GHASEMI B. Effect of melt infiltration parameters on microstructure and mechanical properties of tungsten wire reinforced $(Cu_{50}Zr_{43}Al_7)_{99.5}Si_{0.5}$ metallic glass matrix composite [J]. Transactions of Nonferrous Metals Society of China, 2015, 25: 2624−2629.

[18] CHEN C Q, PEI Y T, HOSSON J T M D. Effects of size on the mechanical response of metallic glasses investigated through in situ TEM bending and compression experiments [J]. Acta Materialia, 2010, 58: 189−200.

[19] WU Y, LI H X, LIU Z Y, CHEN G L, LU Z P. Interpreting size effects of bulk metallic glasses based on a size-independent critical energy density [J]. Intermetallics, 2010, 18: 157−160.

[20] MA W F, KOU H C, LI J S, CHANG H, ZHOU L. Effect of strain rate on compressive behavior of Ti-based bulk metallic glass at room temperature [J]. Journal of Alloys and Compounds, 2009, 472: 214−218.

[21] ZHANG Z F, ZHANG H, PAN X F, DAS J, ECKERT J. Effect of aspect ratio on the compressive deformation and fracture behaviour of Zr-based bulk metallic glass [J]. Philosophical Magazine Letters, 2005, 85: 513−521.

[22] JIANG W H, FAN G J, LIU F X, WANG G Y, CHOO H, LIAW P K. Spatiotemporally inhomogeneous plastic flow of a bulk-metallic glass [J]. International Journal of Plasticity, 2008, 24: 1−16.

[23] BRUCK H A, CHRISTMAN T, ROSAKIS A J, JOHNSON W L. Quasi-static constitutive behavior of $Zr_{41.25}Ti_{13.75}Ni_{10}Cu_{12.5}Be_{22.5}$ bulk amorphous alloys [J]. Scripta Metallurgica et Materialia,1994, 30: 429−434.

[24] SONG M, LI Y Q, HE Y H. Effect of strain rate on the compressive behaviour of a $Zr_{56}Al_{10.9}Ni_{4.6}Cu_{27.8}Nb_{0.7}$ bulk metallic glass [J]. Philosophical Magazine Letters, 2010, 90: 763−770.

[25] GAO X Q, WANG W H, BAI H Y. A diagram for glass transition and plastic deformation in model metallic glasses [J]. Journal of Materials Science and Technology, 2014, 30: 546−550.

[26] ZHANG J, PARK J M, KIM D H, KIM H S. Effect of strain rate on compressive behavior of $Ti_{45}Zr_{16}Ni_9Cu_{10}Be_{20}$ bulk metallic glass [J]. Materials Science and Engineering A, 2007, 449−451: 290−294.

[27] LIU L F, DAI L H, BAI Y L, WEI B C, YU G S. Strain rate-dependent compressive deformation behavior of Nd-based bulk metallic glass [J]. Intermetallics, 2005, 13: 827−832.

[28] XUE Y F, CAI H N, WANG L, WANG F C, ZHANG H F. Effect of loading rate on failure in Zr-based bulk metallic glass [J]. Materials Science and Engineering A, 2008, 473: 105−110.

[29] HUFNAGEL T C, JIAO T, LI Y, RAMESH K T. Deformation and failure of $Zr_{57}Ti_5Cu_{20}Ni_8Al_{10}$ bulk metallic glass under quasi-static and dynamic compression [J]. Journal of Materials Research, 2002, 17: 1441−1445.

[30] MUKAI T, NIEH T G, KAWAMURA Y, INOUE A, HIGASHI K. Dynamic response of a $Pd_{40}Ni_{40}P_{20}$ bulk metallic glass in tension [J]. Scripta Materialia, 2002, 46: 43−47.

[31] MUKAI T, NIEH T G, KAWAMURA Y, INOUE A, HIGASHI K. Effect of strain rate on compressive behavior of a $Pd_{40}Ni_{40}P_{20}$ bulk metallic glass [J]. Intermetallics, 2002, 10: 1071−1077.

[32] BRUCK H A, ROSAKIS A J, JOHNSON W L. The dynamic compressive behavior of beryllium bearing bulk metallic glasses [J]. Journal of Materials Research, 1996, 11: 503−511.

[33] SERGUEEVA A V, MARA N A, KUNTZ J D, BRANAGAN D J, MUKHERJEE A K. Shear band formation and ductility of metallic glasses [J]. Materials Science and Engineering A, 2004, 383: 219−223.

[34] TARIQ N H, AKHTER J I, HASAN B A. Effect of sample geometry on the deformation behavior of Zr-based bulk metallic glass [J]. Journal of Materials Science, 2010, 45: 6170−6173.

[35] JIANG W H, FAN G J, CHOO H, LIAW P K. Ductility of a Zr-based bulk-metallic glass with different specimen's geometries [J]. Materials Letters, 2006, 60: 3537−3540.

[36] CAO Q P, LIU J W, YANG K J, XU F, YAO Z Q, MINKOW A, FECHT H J, IVANISENKO J, CHEN L Y, WANG X D, QU S X, JIANG J Z. Effect of pre-existing shear bands on the tensile mechanical properties of a bulk metallic glass [J]. Acta Materialia, 2010, 58: 1276−1292.

[37] CHEN S H, CHAN K C, XIA L. Effect of stress gradient on the deformation behavior of a bulk metallic glass under uniaxial tension [J]. Materials Science and Engineering A, 2013, 574: 262−265.

[38] CHEN B Q, PANG S J, HAN P P, LI Y, YAVARI A R, VAUGHAN G, ZHANG T. Improvement in mechanical properties of a Zr-based bulk metallic glass by laser surface treatment [J]. Journal of Alloys and Compounds, 2010, 504(S): s45−s47.

[39] WU Hong, LIU Yong, LI Kai-yang, ZHAO Zhong-wei. Casting

effect on compressive brittleness of bulk metallic glass [J]. Transactions of Nonferrous Metals Society of China, 2014, 24: 385−392.

[40] YU P, BAI H Y, ZHAO J G, JIN C Q, WANG W H. Pressure effects on mechanical properties of bulk metallic glass [J]. Applied Physics Letters, 2007, 90: 051906.

[41] CHEN G L, HUI X D, FAN S W, KOU H C, YAO K F. Concept of chemical short range order domain and the glass forming ability in multicomponent liquid [J]. Intermetallics, 2002, 10: 1221−1232.

[42] AN Wei-ke, DING Da-wei, CAI An-hui, ZHOU Guo-jun, LUO Yun, LI Tie-lin, LI Xiao-song. Mechanism, condition and characteristics for the formation of the network structure in Zr−Al−Ni−Cu bulk metallic glasses [J]. Science China: Physics, Mechanics & Astronomy, 2015, 58: 066101.

[43] CAI A H, DING D W, XIONG X, LIU Y, AN W K, ZHOU G J, LUO Y, LI T L, LI X S. Design of Zr−Al−Ni−Cu bulk metallic glasses with network structures [J]. Materials & Design, 2014, 63: 233−237.

[44] CAI An-hui, DING Da-wei, AN Wei-ke, ZHOU Guo-jun, LUO Yun, LI Jiang-hong, PENG Yong-yi. Transition of plasticity and fracture mode of Zr−Al−Ni−Cu bulk metallic glasses with network structures [J]. Transactions of Nonferrous Metals Society of China, 2015, 25: 2617−2623.

[45] SAIDA J, INOUE A. Icosahedral quasicrystalline phase formation in Zr−Al−Ni−Cu glassy alloys by the addition of V, Nb and Ta [J]. Journal of Non-Crystalline Solids, 2002, 312-314: 502−507.

[46] KO H S, CHANG J Y. Effect of short-range order in liquid on the glass forming ability of Fe−Si−B alloy wires [J]. Materials Letters, 2004, 58: 1012−1016.

[47] MILLER M K, SHEN T D, SCHWARZ R B. Atom probe studies of metallic glasses [J]. Journal of Non-Crystalline Solids, 2003, 317: 10−16.

[48] WANG W H. The elastic properties, elastic models and elastic perspectives of metallic glasses [J]. Progress in Materials Science, 2012, 57: 487−656.

[49] ZHAO M, LI M. Local heating in shear banding of bulk metallic glasses [J]. Scripta Materialia, 2011, 65: 493−496.

[50] LEWANDOWSKI J J, GREER A L. Temperature rise at shear bands in metallic glasses [J]. Nature Materials, 2006, 5: 15−18.

[51] KLAUMÜNZER D, MAAß R, DALLA TORRE F H, LÖFFLER J F. Temperature-dependent shear band dynamics in a Zr-based bulk metallic glass [J]. Applied Physics Letters, 2010, 96: 061901.

长径比和加载速率对铜基块体金属玻璃室温力学性能的影响

蔡安辉 [1,2,3]，刘 咏 [2]，吴 宏 [2]，丁大伟 [3]，安伟科 [1]，周果君 [1]，罗 云 [1]，彭勇宜 [4]，李小松 [1]

1. 湖南理工学院 机械工程学院，岳阳 414000；
2. 中南大学 粉末冶金国家重点实验室，长沙 410083；
3. 中国科学院 物理研究所，北京 100190；
4. 中南大学 物理与电子学院，长沙 410083

摘 要：通过单向压缩实验在试样长径比(H/D)和加载速率分别为 1:1~2.5:1 和 1×10^{-5}~1×10^{-2} s^{-1} 的条件下对 $Cu_{50}Zr_{40}Ti_{10-x}Ni_x$ ($0\le x\le 4$，摩尔分数，%) 块体金属玻璃的室温力学性能进行了系统研究。在长径比为 1:1 的情况下，当加载速率为 1×10^{-4} s^{-1} 时，$Cu_{50}Zr_{40}Ti_{10}$ 块体金属玻璃表现出超塑性；而 $Cu_{50}Zr_{40}Ti_{10-x}Ni_x$ (x=1~3，摩尔分数，%) 块体金属玻璃在加载速度为 1×10^{-2} s^{-1} 的条件下出现超塑性；塑性应变(ε_p)、屈服强度(σ_y)和断裂强度(σ_f)显著地依赖于长径比和加载速率；当加载速率为 1×10^{-2} s^{-1} 时，长径比为 1:1 的块体金属玻璃的屈服强度几乎与其他长径比的块体金属玻璃的断裂强度接近；另外，本文作者也探讨了铜基块体金属玻璃力学性能对加载速率和长径比的响应机理。

关键词：铜基块体金属玻璃；长径比；加载速率；塑性；强度

(Edited by Wei-ping CHEN)